Local Deformation in Carbon Black-Filled Polyisoprene Rubbers Studied by NMR and X-ray Diffraction

Stéphane Dupres, Didier R. Long,† Pierre-Antoine Albouy, and Paul Sotta*,†

Laboratoire de Physique des Solides, CNRS/Université Paris-Sud, UMR 8502, 91405 Orsay Cedex, France

Received January 4, 2009; Revised Manuscript Received February 22, 2009

ABSTRACT: We study polyisoprene elastomers reinforced with carbon blacks (CBs) of various grades. In addition to mechanical characterization at medium/large elongation ratios, we use deuterium NMR experiments on stretched samples to measure the local strain within the elastomer matrix and X-ray scattering to measure the onset of strain-induced crystallization in the reinforced systems. We show that NMR experiments and measurements of the onset of crystallization are indeed sensitive to the different degrees of reinforcement observed according to the various CB grades and volume fractions. The measurements show a good correlation between macroscopic (mechanical) and microscopic (NMR, crystallization) measurements. This indicates that the techniques used here are valuable techniques for characterizing reinforced systems in which fillers have complex morphologies and dispersion states. The discrepancies between the results of both macroscopic and microscopic measurements are analyzed. The local strain as measured by NMR is lower than the macroscopic strain. This indicates the presence of some degree of local strain (or stress) inhomogeneity within the elastomer matrix in the reinforced systems. This inhomogeneity is more pronounced in the presence of more reinforcing carbon black grades.

I. Introduction

Elastomers reinforced by the inclusion of solid particles or aggregates show remarkable mechanical properties.[1] First, they exhibit a strong reinforcement, as measured by the ratio of the elastic modulus of the material to that of the pure, unfilled matrix, which may be as large as a factor 100 in a limited temperature range just above T_g, and it extends over a broad temperature range with smaller values, however. In practical applications, reinforced elastomers are often used in this broad temperature range. Reinforcement itself coexists with a strong nonlinear drop of the elastic modulus (known as Payne effect), irreversibility, and long-time relaxation, and an outstanding resistance to tear and wear.[2,3] Filled rubbers of practical interest are commonly reinforced with carbon black (CB) aggregates, which exhibit fractal structures with various morphologies.[4−6]

Although mechanical reinforcement by carbon black aggregates has been known and extensively characterized for almost a century, microscopic mechanisms are still far from being fully understood, and a number of questions remain largely under debate.[7] Several mechanisms have been proposed to explain both reinforcement and nonlinear effects. The Guth and Gold model relates the elastic modulus to the filler volume fraction in a way that is analogous to the Einstein model for the viscosity of a suspension of particles[8] in the linear regime. The concept of local strain (or equivalently stress) amplification has been used in a number of studies as a possible explanation for the reinforcement.[9−11] In such models, the local strain within the rubbery matrix is amplified because of the presence of a rigid fraction of material (fillers) as well as a fraction of the elastomer matrix screened from the overall strain in the case of fractal, structured reinforcing aggregates (the so-called occluded rubber fraction).[6] Perfect cohesion is generally assumed at the matrix/filler interfaces. A relation between strain amplification and filler volume fraction was proposed and tested quantitatively by small-angle neutron scattering (SANS) in model cross-linked thermoplastic elastomers with PS spheres used as fillers within a PI matrix[12] in a range of λ between 1.0 and 2.0. It was shown that the filler spheres undergo affine displacement and that in this model system the strain amplification measured in the PI matrix chains fits with a geometrical model. In an unfilled cross-linked PI network, it was shown that the affinity holds down to the scale of the network strands.[13]

Reinforcement has also been described by a double network (or "supernetwork") model in which a fraction of the elastomer chains tightly bound to fillers form a secondary, large-scale network of elastomer strands between fillers acting as cross-links.[14,15] A submicrometric approach has been developed recently in which a "virtual rubber" is constructed on the basis of a realistic representation of the 3D spatial distribution of CB aggregates, as measured by 3D TEM.[16,17] The distribution of local strain can then be computed in the reconstructed material submitted to a macroscopic strain by finite element modeling,[18] assuming that the constitutive law of the elastomer matrix remains unaffected by the fillers.

However, all of these models essentially correspond to geometrical descriptions in which the fraction of the sample that does not deform is given by the fraction of solid filler particles or aggregates plus the fraction of occluded rubber and perhaps an adsorbed elastomer layer with dynamical properties strongly affected with respect to the bulk,[19] which may also contribute to an increase in the undeformed fraction of the material. Such models can certainly not account for the strong temperature variation of the mechanical properties, specifically the huge increase in reinforcement in the vicinity of the elastomer matrix glass transition. Nevertheless, the various mechanisms described in these models may play a role in the higher temperature range, which often effectively corresponds to the application range, as mentioned above.

However, several mechanisms have been proposed to explain nonlinear effects and dissipative properties: desorption/absorption of polymer chains at the filler surface;[20] destruction/reformation of the network formed by fillers,[21,22] specifically when fractal aggregates are used,[23] or networking of fillers surrounded by bounded polymer;[24−26] and disentanglement of the bulk rubber matrix from the bounded chains.[27] Nonaffinity and particle reorganization as well as the role of disorder were

* Corresponding author. E-mail: paul.sotta-exterieur@eu.rhodia.com.
† Present address: Laboratoire Polymères et Matériaux Avancés, CNRS/Rhodia Recherches et Technologies, UMR 5268, 85 rue des Frères Perret, 69192 Saint-Fons Cedex, France.

10.1021/ma900006y CCC: $40.75
Published on Web 03/18/2009

also considered[16] to explain the Payne effect and other nonlinear and irreversible phenomena.[28]

There is relatively little direct experimental evidence of these mechanisms, which are very difficult to distinguish from each other on a microscopic scale. Also, the related parameters are difficult to control independently.

A model based on the presence of glassy layers related to the shift in the T_g matrix in the vicinity of the filler surface has been proposed recently.[29−31] On the basis of the measurements performed in polyacrylate matrices reinforced with well-dispersed, monodisperse silica particles, the reinforcement could be modeled by considering an effective solid fraction including a rigid (glassy) polymer layer around filler particles,[30,32,33] which was measured directly by NMR. By considering the temperature variation of the glassy layer thickness, a new time−concentration−temperature superposition law for reinforced elastomers was proposed.[30] In practice, however, in elastomers reinforced by aggregates that have a complex structure and interact in a complex way, overlapping of glassy layers may have to be considered in the temperature−concentration master curve proposed from the study of model systems in ref 30. In some other cases, it was argued that this layer of restricted mobility is not the dominant effect on reinforcement.[35]

Therefore, altogether, there is clearly a need to relate reinforcement properties to the nature and morphology of the reinforcing system with regards to the volume fraction of fillers and their morphology in the medium-to-large strain regime. This demands correlating characterization of the macroscopic behavior to microscopic investigations in systems reinforced with fillers that are perhaps quite complex. In this article, we address the question of how the stress is transmitted on a microscopic scale in elastomers filled with CB aggregates. As the strain amplitude is increased, several distinct regimes are observed in the mechanical response. The Payne effect,[21] which occurs between 1 (or a few) % strain typically and a few 10%, is characterized by a large drop in the storage modulus and correlatively, a peak in the loss modulus. We focus here on a medium to large range of deformation, beyond the Payne effect. This regime has not been studied much quantitatively, even though it is very important in applications of reinforced rubbers. The bulk deformation of a tire typically amounts to 10 to 20%, and the deformation may be much higher than that locally, for instance in the tire tread. Strain-induced crystallization is another important phenomenon that occurs in this range of deformation. It is most pronounced in natural rubber, but it also occurs in some synthetic rubbers, such as polyisoprene, provided that the stereoregularity is high enough. It leads to self-reinforcement by crystallites and to extremely high ultimate properties, such as resistance to tear and abrasion wear.

We study CB-filled synthetic polyisoprene elastomers with formulations close to industrially used systems. As control parameters, we used CB of different grades, that is, various fineness (size of primary particles) and morphologies and with various volume fractions.

Understanding the various mechanisms associated with reinforcement implies combining techniques that give access to complementary information. Here we combine three independent measurements of the elastic properties on different scales. First, we characterize macroscopic elastic properties by measuring large amplitude elongation stress−strain curves. Then, we probe the local strain within the polymer matrix by using deuterium NMR. It has been shown that deuterium NMR gives direct access to local chain stretching, which in turn is directly related to the local strain, or equivalently to the density of elastic energy stored on the scale of polymer chain within the rubbery matrix.[36,37] Then, we determine the onset of strain-induced crystallization by X-ray diffraction.

Table 1. Characteristics of the CB Used[a]

CB grade	N_2 adsorption (10^3 m^2/kg)	R (nm)	DBPA (10^{-5} m^3/kg)
N358	80	28	150
N326	78	28	72
N772	32	75	65

[a] R is the primary particle diameter.

We discuss the results in terms of local strain amplification, which provides here an appropriate way to discuss the differences in strain/stress behavior observed on various scales using different techniques and which allows us to discuss the differences obtained from the three independent measurements. We relate these differences to the inhomogeneities of the local stress (or strain). We compare these inhomogeneities in the presence of CB of various grades.

The article is organized as follows. In Section II, we present the systems used in this study and give some basics on the techniques that are used to monitor the rubbery matrix on a microscopic scale. We present and discuss the results in Section III.

II. Experimental Section

A. Samples. The samples (kindly supplied by Manufacture Francaise des Pneumatiques Michelin, Ladoux, France) have been obtained by sulfur vulcanization of synthetic *cis*-1,4-polyisoprene (synthetic rubber (SR), commercial denomination SKI 3). SR is not perfectly regular and contains a few *trans*-1,4 and *trans*-3,4 monomers (overall amount 1.5 to 2%), which alters, but does not completely suppress, strain-induced crystallization as compared with natural *cis*-1,4 polyisoprene (natural rubber). The samples were prepared by mill-compounding the vulcanization additives and carbon fillers into the rubber using classical Brabender dispersion and then curing the systems under standard conditions. We use three different grades of carbon blacks (N358, N326, and N772) with primary particle sizes ranging from 28 (N326 and N358) to 75 nm (N772).[38] The characteristics of the CBs are summarized in Table 1. The primary particle size ("fineness" of the CB) is determined from nitrogen surface area. The structure is determined from dibutylphthalate absorption (DBPA), which indicates that N358 is more structured; that is, it has a less-compact morphology with more branching, larger pores, or both inside the aggregates than N326.[39] We use two different CB fractions (30 and 50 phr, corresponding to volume fractions of 0.143 and 0.217, respectively) and three sulfur/accelerator contents (1.0, 1.5, and 2.5 phr sulfur), which correspond to various cross-link densities, for each CB grade. Samples are listed in Table 2. Test samples used in mechanical and X-ray diffraction experiments were dumbbells of typical dimensions: $L_0 = 12.5$ mm long, 2 mm thick, and 5 mm wide.

The shear modulus in the linear regime was measured for some of the samples at $T = 23$ °C with an ARES rheometer in plane−plane geometry, at 1 rad·s^{-1} frequency and 0.1% amplitude. The samples were 2 mm thick disks of 8 mm in diameter glues on the rheometer plates with a cyanoacrylate (Loctite) glue. The values of the shear modulus, G', are reported in Table 2, and the corresponding values of reinforcement, R, in the linear regime with respect to the same unfilled reference sample 1, defined as the ratio G'/G'_0 (where G'_0 is the modulus of sample 1), are reported in Table 4.

Quantitative characterization of CB aggregate dispersion is not easily accessible in the samples. Small or ultrasmall angle scattering is impeded by the presence of zinc oxide particles. Cryomicrotomed lamellae for TEM tend to crumple at room temperature. Therefore, the dispersion of CB aggregates was checked qualitatively by high-resolution field emission gun (FEG) SEM (Hitachi). The accelerating voltage was 5 kV. The surface of the samples was carefully washed with ethanol. No metalization was used. A representative SEM picture of the dispersion obtained in sample 8 (50 phr N358) is shown in Figure 1. The images obtained in all samples show

Table 2. List and Characteristics of the Samples[a]

sample	CB grade	c	Φ	ϕ_s	G' (MPa)
1	unfilled	~0	~0	1.5	0.48
2	N326	50	21.7	2.5	4.3
3		50	21.7	1.5	3.5
4		50	21.7	1.0	3.0
5		30	14.3	2.5	1.6
6		30	14.3	1.0	1.45
7	N358	50	21.7	2.5	4.8
8		50	21.7	1.5	3.8
9		50	21.7	1.0	3.0
10		30	14.3	2.5	2.2
11		30	14.3	1.0	1.8
12	N772	50	21.7	2.5	1.8
13		50	21.7	1.5	1.4
14		50	21.7	1.0	
15		30	14.3	2.5	
16		30	14.3	1.0	

[a] c is the CB content in phr, Φ is the CB volume fraction in percent, and ϕ_s is the sulfur (accelerator) content in phr (sulfur and accelerator are in equal amounts in phr). In addition, all samples contain 3 phr ZnO and identical quantities of other additives. G' is the shear modulus measured at 23 °C, 1 rad·s $^{-1}$ frequency, and 0.1% amplitude.

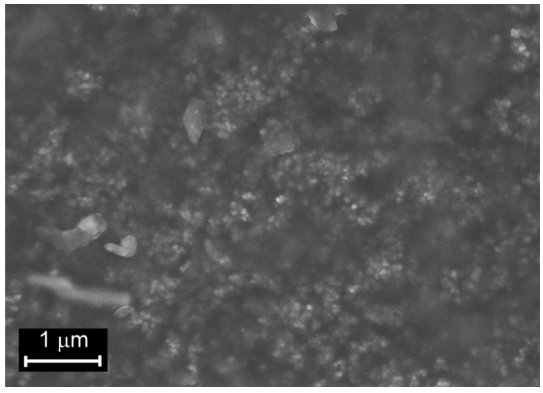

Figure 1. High-resolution field emission gun (FEG) SEM image obtained in sample 8 (50 phr N358), showing the dispersion of CB aggregates on a mesoscopic scale.

good dispersion down to a scale on the order 100 nm, which is the typical size of CB aggregates. No micrometric agglomerates were detected. Close inspection of the pictures shows aggregate clustering/chaining with an apparent nearer neighbor distance of a few tens of nanometers and voids on the order of 200 to 500 nm. This compares well to what is usually observed in elastomers reinforced with well-dispersed CB aggregates.[16]

B. Mechanical Measurements. Mechanical measurements were performed with a homemade stretching device that controls the displacement and measures the force. All measurements are done at room temperature. Samples are stretched uniaxially at a typical given rate of $dL/dt = L_0\dot{\epsilon} = 0.08$ mm/s. The resolution in elongation is 3 μm. The elongation ratio is defined as $\lambda = L/L_0 = \epsilon + 1$ (ϵ is the deformation). The true stress, σ_v, is computed from the measured nominal stress σ, as $\sigma_v = \lambda\sigma$. In the following, we have chosen to plot the true stress, σ_v, as a function of the strain function, Λ, defined as

$$\Lambda = \lambda^2 - \lambda^{-1} \tag{1}$$

as is usually done in rubber elasticity. Note that the large amplitude deformation cycles shown in Section IIIA as well as NMR and X-ray diffraction results are obtained in as-prepared samples.

C. Deuterium Nuclear Magnetic Resonance Experiments. Deuterium Nuclear Magnetic Resonance (NMR) measurements were performed on a homemade spectrometer operating at a deuterium resonance frequency of 61.4 MHz with a 9.4 T Oxford magnet (proton frequency, 400 MHz) and a static Bruker probe. We use a standard $\pi/2$ sequence with a 90° pulse length of approximately 4.8 μs and recycle delay of 1.2 s. The samples are $30 \times 3 \times 1$ mm^3 stripes that are elongated within the NMR measuring probe by a screw bolt system in a closed 5 mm glass tube placed in the NMR coil. The stretching direction is parallel to the static magnetic field, B_0. Samples have been elongated to a typical deformation ratio ranging from $\lambda = 1$ (reference, undeformed state) to 3, as determined from the distance between two marks on the sample measured with a stereomicroscope before and after NMR acquisition.

Deuterium (^{2}H or D) NMR has been extensively used to study the orientational order induced in rubber network under uniaxial stress.[40] It was shown that deuterium NMR gives access to the local chain stretching, which is directly related to the elastic energy stored in the rubbery matrix on the scale of network chains.[36,37] The approach used here consists of introducing within the elastomer matrix a small amount (typically 2 wt %) of a perdeuterated solvent (D_{12}-cyclohexane or D_{26}-dodecane), which is used as a probe of the local anisotropy within the matrix.[41] It is supposed that the matrix properties are not significantly affected by the presence of solvent. It was shown that the motion of solvent molecules is coupled to the average anisotropy induced in the stretched elastomer matrix (with a proportionality coefficient that depends on only the polymer/solvent pair).[41]

In an anisotropic medium, the quadrupolar interaction is partially time-averaged by rapid molecular motions, and it differs from zero because the orientation fluctuations of the C$-^2$H bonds are anisotropic on the typical time scale of 10^{-5} s. Therefore, for motions uniaxial around a symmetry axis, which is the case in a uniaxially stretched sample, the deuterium resonance line is split in a doublet with a splitting (in frequency units) $\Delta = \omega_Q S$, where S is the orientational order parameter of the considered C$-^2$H bond and ω_Q is the magnitude of the quadrupolar interaction (~125 kHz in hydrocarbon molecules). According to classical elasticity theory, the average anisotropy in the elastomer matrix is related to the cross-link density and to the local extension, and the order parameter, S, of solvent molecules[36] for an anisotropy direction parallel to the manetic field B_0 reads

$$S = \nu\frac{R^2}{N^2a^2}\Lambda \approx \frac{\nu}{N}\Lambda \tag{2}$$

in which N is the average number of monomers or, more precisely, statistical segments, between cross-links ($1/N$ is the cross-link density), a is the monomer size (on the order of, say, 0.5 nm), R^2 is the average squared end-to-end vector of network chains (between cross-links), and ν is a parameter related to the orientational coupling of chain segments to the solvent molecules on the order of 0.2 to 0.3.[41]

It follows that in an unfilled elastomer (described by entropic elasticity) the solvent doublet splitting, Δ, varies linearly with the strain function, $\Lambda = \lambda^2 - \lambda^{-1}$, which is the natural parameter describing uniaxial elongation in an affinely deformed elastomer network. Accordingly, we choose here to plot the splitting, Δ, as a function of the strain function, Λ.

D. X-ray Scattering. A homemade stretching machine mounted on an X-ray rotating anode generator (Cu Kα wavelength: λ_α = 0.1542 nm) is used. Collimation reduces the beam diameter to ca. 0.2 mm. The displacement and the force are measured during in situ drawing experiments. The experimental setup for monitoring the onset of crystallization was described in detail in ref 42. Two-dimensional diffraction patterns were collected by photostimulated image plates. A typical diffraction pattern obtained in the nonreinforced sample at large elongation is shown in Figure 2. Three diffraction rings due to zinc oxide crystals embedded in the rubber are visible at large angle. However, the weak reflection at low angles corresponds to the (003) reflection of the crystallized stearic acid.

The large diffuse ring is due to the polymer amorphous fraction. The anisotropy observed in the diffuse ring intensity indicates that

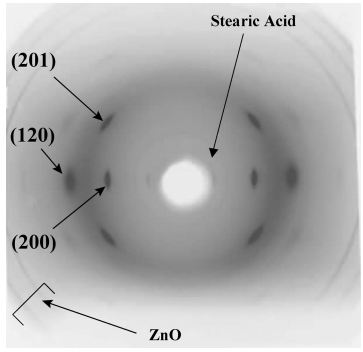

Figure 2. Typical X-ray diffraction spectrum from a sample (sample 7) stretched at $\lambda = 5$. The drawing direction is vertical. Indexation of the various crystalline peaks is indicated. Crystalline diffraction at low q is due to stearic acid, as indicated.

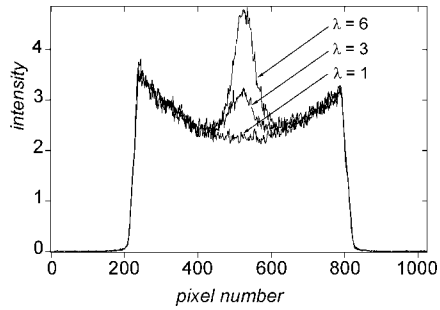

Figure 3. Intensity (in linear arbitrary units) measured in the linear counter centered on the 200 Bragg peak of the crystallites (and placed horizontally on the spectrum shown in Figure 2). Spectra obtained at various elongation ratios, λ, are calibrated to superpose the background so as to measure the extra intensity of the diffraction peak.

polymer chains within the amorphous phase, or at least a significant fraction of them, are quite strongly oriented.[43]

Crystallization occurs as samples are stretched at relatively high elongation. Bragg reflections indicate that crystallites are highly oriented. The apparition and evolution of the (200) Bragg reflection of polyisoprene is monitored as a function of elongation to estimate the onset of crystallinity. This Bragg reflection has been chosen to avoid overlap with the amorphous ring. A linear detector centered on the (200) reflection and placed vertically (i.e., horizontally on the pattern in Figure 2) is then used for quantitative measurements. As the rubber matrix starts to crystallize, the (200) reflection peak appears on top of the background (Figure 3). To extract the peak intensity, the spectra are normalized to obtain equal backgrounds, and the peak intensity is measured as the total area under the peak, computed after substracting the normalized background and corrected for sample absorption. This process is illustrated in Figure 3. Samples are drawn continuously at a speed of $\dot{\lambda} = 1.2 \times 10^{-3}$ s^{-1}. The acquisition time is 10 s.

III. Results

We first present the mechanical measurements. We concentrate here on the medium/large regime of deformation. To get more microscopic insight into the system by more directly checking the strain on a microscopic scale within the elastomer matrix, we have performed deuterium NMR experiments in the same series of samples. NMR results are presented in Section IIIB. X-ray measurements of the onset of strain-induced crystallization have been performed with a two-fold purpose. First, strain-induced crystallization may play a role in relaxing part of the stress in the rubber matrix and thus may be responsible for lower values of the effective, measured strain amplification factor. It is thus essential to check whether the samples crystallize in the range of elongation investigated.

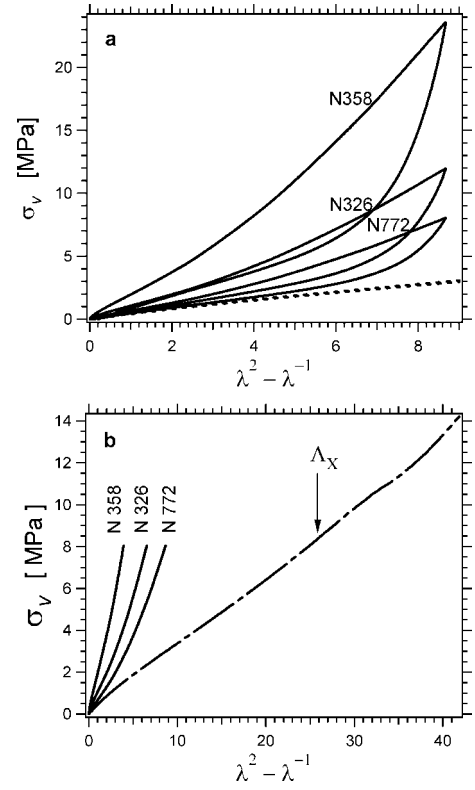

Figure 4. (a) Stress−strain elongation cycles (the true stress as a function of the elongation parameter, $\Lambda = \lambda^2 - \lambda^{-1}$) in samples 1 (reference, unfilled sample), 3 (N326), 8 (N358), and 13 (N772) measured at $T = 22$ °C and strain rate of 1 mm/s (which corresponds to $\dot{\lambda} = 0.08$). This illustrates the effect of the carbon black morphology on reinforcement properties. (b) Full range of strain (or stress) in which the amplification factor, f, is computed, that is, up to a stress of ~8 MPa, which roughly corresponds to the onset of strain-induced crystallization in the nonreinforced sample (indicated as Λ_X in the graph). Only the stretching parts of the cycles are shown.

Table 3. P: NMR Slopes, $P = \Delta\nu/(\lambda^2 - \lambda^{-1})$, Measured in the Various Samples Swollen with 5% Deuterated Cyclohexane[a]

sample no.	CB grade	c	ϕ_s	P (Hz)	Λ_X
1	unfilled		1.5	54	26.0
2	N326	50	2.5	117	4.4
3		50	1.5	88	6.4
4		50	1.0	66	8.5
5		30	2.5	82	6.7
6		30	1.0	52	8.6
7	N358	50	2.5	112	3.9
8		50	1.5	98	4.4
9		50	1.0	57	6.8
10		30	2.5	83	6.2
11		30	1.0	51	7.8
12	N772	50	2.5	108	8.3
13		50	1.5	78	8.9
14		50	1.0	85	9.3
15		30	2.5	97	8.7
16		30	1.0	64	10.9

[a] $\Lambda_X = \lambda_X^2 - \lambda_X^{-1}$: elongation parameter at the onset of crystallinity.

Second, the onset of crystallization by itself, as compared with that in the nonreinforced reference sample, may give a measurement of the local strain in reinforced samples within a strain amplification picture. Results of crystallization measurements will be presented in Section IIIC. Both NMR and X-ray measurements give access to the local strain in the rubber matrix. Therefore, a proper way to analyze and compare the various data is to compute the "strain amplification factor", which is obtained by comparing the elongation ratio measured in a reinforced sample at a given level of stress to that in a nonreinforced sample, which is taken as a reference.

A. Results of Mechanical Measurements. Examples of large amplitude stress−strain cycles obtained in elongation at room temperature are shown in Figure 4a in both a nonreinforced sample (sample 1) and for samples filled with 50 phr of CB of different grades (volume fraction 20%), with all samples having the same rubber matrix, that is, vulcanized under the same conditions with the same sulfur/accelerator content of 1.5 phr (samples 3, 8, and 13). As mentioned above, we investigate the behavior of as-prepared samples, and we have chosen to plot the true stress as a function of the elongation parameter, $\Lambda = \lambda^2 - \lambda^{-1}$.

The curves in Figure 4a illustrate the effect of the CB morphology on reinforcement properties. As expected, the obtained reinforcement, that is, the enhancement of stress in filled samples as compared with the unfilled reference sample, is higher for smaller primary particles, more structured CB aggregates, or both.

Reinforcement of elastomers filled with solid particles/aggregates has often been analyzed in terms of "local strain amplification",[9−11] by comparing the strain measured in a reinforced sample to that in a reference (unfilled) sample at the same value of the stress (or of some other measured quantity, as proposed below). This strain amplification representation provides a simple way to analyze measurements, quantify the reinforcement, and assess differences between results obtained by different techniques in various samples. This representation of the data is used here to allow a comparison of results from different experiments that give access to the local strain. It is used to compare a series of samples with a given arbitrary reference sample rather than to quantify the effect of fillers in a given sample.

Strain amplification factor is computed from stress−strain curves as the ratio of the elongation parameter, $\Lambda = \lambda^2 - \lambda^{-1}$, measured in each reinforced sample to the value Λ_m measured in the reference unfilled sample at the same stress value. (Λ_m may be considered to be the microscopic strain within the elastomer matrix of the reinforced system, amplified with respect to the macroscopic measured strain Λ.) The strain amplification function, f, is then defined by

$$f = \frac{\Lambda_m}{\Lambda} \tag{3}$$

The elongation range considered here is illustrated in Figure 4b (same data as in Figure 4a), which shows the full range in which the amplification factor, f, is computed. The upper limit is chosen to be close to the onset of crystallization, which occurs at about $\lambda \approx 5$ (or $\Lambda_X \approx 25$) in the nonreinforced sample. (See Section IIIC and Table 3.) Only upward (stretching) parts of the cycles shown in Figure 4a are used to compute f and are shown in Figure 4b. In Figure 4b, the stress softening associated with crystallization is clearly visible around $\Lambda \approx 30$ on the curve of the unfilled sample.

The strain amplification functions, f_{mec}, computed from the data in Figure 4b, are plotted as a function of the macroscopic elongation parameter, Λ, in Figure 5 in the three samples reinforced with various CB grades. There are two distinct regimes in these curves. The steep decrease in the stress amplification factor at small elongation amplitudes corresponds to the Payne effect; that is, to the steep decrease in reinforcement for strain amplitudes between 0 and a few 10%. Note that the experimental curves in Figure 5 are not precise at small elongation because of the uncertainty in determining the zero stress point in elongation experiments. (A small stress value on the order of 0.1 N is applied prior to starting the elongation.) In this range, the factor f increases progressively as λ increases.

The amplification functions, f_{mec}, measured in all samples from mechanical measurements, are reported in Table 4. The values at the minimum of the curves f versus Λ are reported. All samples, whatever their cross-link densities, are compared with the same nonreinforced sample (sample 1) taken as a reference. Note again that this is somewhat different from what is usually done to study specifically the effect of fillers in terms of strain amplification. The results of mechanical measurements will be discussed in Section IV.

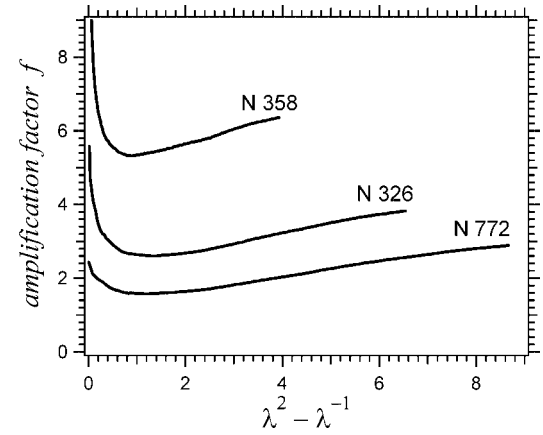

Figure 5. Strain amplification function, f, defined as the ratio $f = (\lambda_m^2 - \lambda_m^{-1})/(\lambda^2 - \lambda^{-1})$ from the curves in Figure 4. In each reinforced sample, for a macroscopic elongation, λ, measured at a stress, σ_t, λ_m is the elongation measured in the nonreinforced sample 1 at the same level of stress. For each sample, the function f is plotted versus the macroscopic elongation parameter $\Lambda = \lambda^2 - \lambda^{-1}$. Beyond $\Lambda \approx 0.5$ to 1.0, f is approximately constant. At small Λ values, the steep decay corresponds to the Payne effect.

Table 4. Amplification Factors, f (as Defined in Equation 3), Measured in the Various Samples from Deuterium NMR Slopes (f_{NMR}), from Stress Measurements (f_{mec}), and from the Onset of Crystallinity (f_x) (See Table 3)[a]

sample	CB grade	c	ϕ_s	R	f_{NMR}	f_{mec}	f_x
1	unfilled		1.5	1	1	1	1
2	N326	50	2.5	9.0	2.15	4.2	5.9
3		50	1.5	7.3	1.6	2.87	4.0
4		50	1.0	6.3	1.2	2.55	3.1
5		30	2.5	3.3	1.46	3.0	3.9
6		30	1.0	3.0	0.96	1.7	3.0
7	N358	50	2.5	10.0	2.07	6.0	6.6
8		50	1.5	7.9	1.82	5.51	5.9
9		50	1.0	6.3	1.05	3.8	3.8
10		30	2.5	4.6	1.51	3.6	4.2
11		30	1.0	3.8	0.93	3.2	3.3
12	N772	50	2.5	2.9	1.54	2.8	3.1
13		50	1.5	2.5	1.44	2.0	2.9
14		50	1.0		1.27	2.15	2.8
15		30	2.5		1.36	2.49	3.0
16		30	1.0		1.19	1.8	2.4

[a] c is the CB content in phr, ϕ_s is the sulfur/accelerator content in phr, and R is the reinforcement of the shear modulus in the linear regime, defined as the ratio G'/G'_0, where G'_0 is the modulus of the unfilled reference sample.

B. Nuclear Magnetic Resonance Results. Representative deuterium NMR spectra obtained in D_{26}-dodecane introduced in samples stretched to $\lambda = 2$ are shown in Figure 6. The spectra obtained in stretched samples (spectra b and d) exhibit characteristic doublet structures that indicate that solvent molecules undergo anisotropic reorientational motions within the stretched samples.

The spectra obtained in D_{12}-cyclohexane molecules exhibit one single doublet because all 12 deuterons in the perdeuterated molecule are equivalent. In D_{26}-dodecane, deuterons are not equivalent. Two doublets appear, one from $-CH_3$ and one from $-CH_2$ groups. The splitting of the doublet from $-CH_3$ is smaller than that from $-CH_2$ groups by a factor on the order of 4.5.

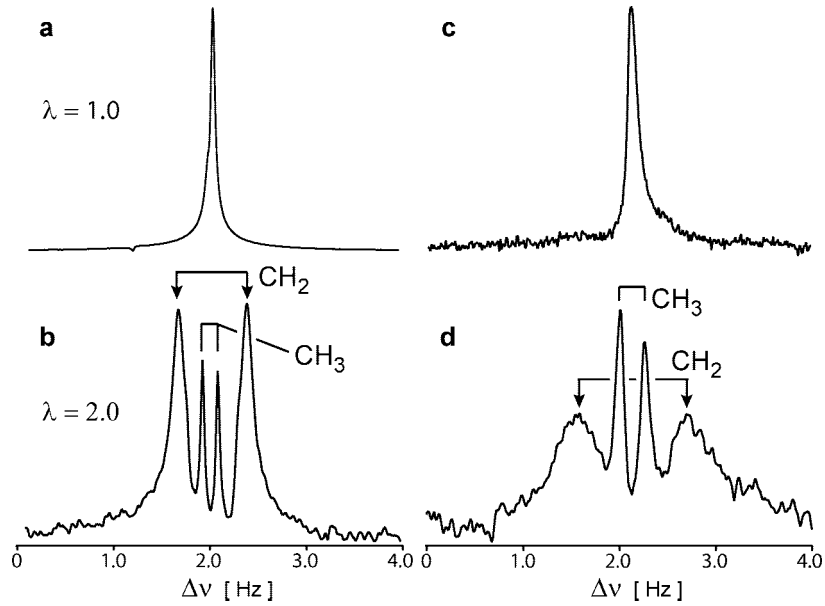

Figure 6. Representative examples of ^{2}H NMR spectra of D_{26}-dodecane at room temperature: (a,c) relaxed samples, (b,d) samples uniaxially stretched to $\lambda = 2$, (a,b) nonreinforced reference sample, and (c,d) sample 8 reinforced with 50 phr N358. The dodecane concentration is 2 wt % polymer. Note that only one doublet would be observed in cyclohexane, in which all ^{2}H are equivalent.

Two effects contribute to this factor. First, rotation of methyl groups around their axis decreases the splitting value by a geometrical factor of 1/3. Then, it is likely that the orientational order along the stretching direction decreases from the center of the molecule toward the extremities. $-CH_3$ lines are extremely narrow because all deuterons in $-CH_3$ groups are equivalent. The lines in the $-CH_2$ doublet are broader because they include contributions from all $-CH_2$ groups along the chain, which may have slightly different average orientations.

Spectra obtained in D_{26}-dodecane at a similar stretching ratio in nonreinforced and reinforced samples, respectively, are compared in Figure 6. The relatively modest line broadening observed in the presence of fillers indicates that the dynamics of solvent molecules is not strongly affected in the presence of fillers. Actually, the observed line broadening may essentially be attributed to magnetic heterogeneities related to CB paramagnetism.[44] This suggests that the dynamics is not drastically affected in the presence of fillers in the rubber matrix, or at least in most of it. However, the superposition of signals with very different splittings coming from mobile regions with different local elastic energy (inhomogeneities of the local strain) would lead to a pronounced broadening of NMR lines as well. This is not observed, which means that solvent molecules are ale to average local inhomogeneities by diffusing through the matrix, which results in a single narrow (even though slightly broadened) NMR line. This is a further indication of solvent molecules retaining a fast dynamics in the presence of fillers.

The NMR splittings, Δ, are plotted in Figure 7 as a function of the elongation parameter, $\Lambda = \lambda^2 - \lambda^{-1}$, for the same samples as those in Figure 4 reinforced with different CB grades, together with the corresponding nonreinforced sample. It is observed that Δ is a linear function of Λ in all samples. No significant induced crystallization occurs in the range of elongation investigated. (See Section IIIC). Indeed, it was observed that the NMR splitting tends to become constant as crystallization starts because crystallization results in relaxing the stress within the amorphous parts of the matrix.[49]

The slope $P = \Delta/\Lambda$ is related to the average microscopic degree of strain in the rubber matrix, according to eq 2. To check the consistency of the approach, it is important to compare the values obtained from mechanical and NMR measurements in the nonreinforced sample quantitatively. Within the classical

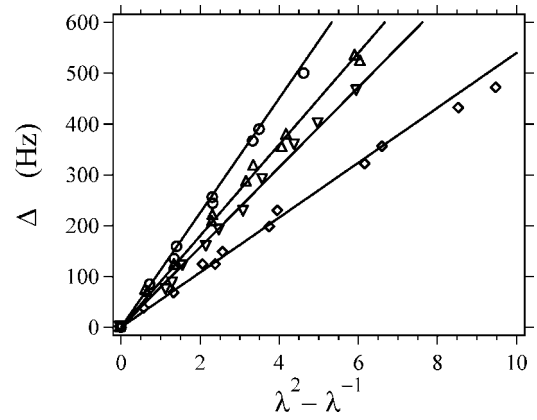

Figure 7. Examples of plots of the ^{2}H NMR splitting, Δ, versus the elongation parameter, $\Lambda = \lambda^2 - \lambda^{-1}$, in various samples swollen with 2% deuterated cyclohexane: ◇, nonreinforced sample 1; ▽, sample 13 (N772); △, sample 3 (N326); ○, sample 8 (N358) (the same samples as in Figure 4). Each set of data results from two independent experiments on two different test samples of each index numbering. Lines are approximate linear fits to the data.

entropic elasticity picture for a pure rubber, the shear modulus may be written as $G' = \sigma_t/\Lambda = (k_BT)/(Na^3)$, and the NMR slope may be written as: $P = \Delta/\Lambda = (2/5)((\omega_Q\nu)/N) = (2/5)((\omega_Q\nu)/(k_BT))G'a^3$, where N denotes the average number of monomers between cross-links, a^3 is the monomer volume (on the order of 1.2×10^{-28} m^3), and ν is a coupling constant between solvent molecules and polymer chain segments on the order of 0.2 to 0.3.[37] In the case of cyclohexane, the effective quadrupolar constant, ω_Q, is on the order of 31×10^3 Hz.[45] With $G' \cong 3.5 \times 10^5$ Pa (Figure 4), we obtain $P \approx 50$ Hz, which is indeed the order of magnitude of the measured value. This indicates that the local anisotropy in chain segments, as measured by NMR (corresponding to an average level of strain on the scale of network chains), indeed quantitatively corresponds to the macroscopic stress in the unfilled sample within an entropic elasticity picture, that is, with an elastic free energy on the order of k_BT per chain under stretching. Then, an important question to understand reinforcement is to check whether this remains true in reinforced elastomers.

As mentioned before, Figure 7 shows that the splitting, Δ, varies linearly as a function of $\Lambda = \lambda^2 - \lambda^{-1}$ in reinforced samples as well as in the nonreinforced reference sample. From the measured slopes, an amplification factor, f_{NMR}, may be defined for each reinforced sample as the ratio of its NMR slope, P, to that of a reference nonreinforced sample, P_0

$$f_{NMR} = \frac{P}{P_0} = \frac{\Lambda_m}{\Lambda} \quad (4)$$

where Λ_m is the strain function measured in the nonreinforced sample at the same splitting value, Δ. In the language of strain amplification, Λ_m would be considered to be the average local (microscopic) elongation ratio corresponding to the macroscopic elongation ratio, Λ. This definition may be applied to the comparison of the NMR slopes in any pair of samples. Here all samples are compared with the same reference sample (sample 1) in the same way as in Section IIIA.

The linear variation and thus constant factor, f_{NMR}, observed in Figure 7 is in qualitative agreement with the curves shown in Figure 5, which show a slowly increasing f_{mec} factor in the medium/high elongation range. The NMR data in Figure 7 are not precise enough to discriminate either type of behavior. Note that the Payne effect, observed in the curves in Figure 5 at smaller elongations, cannot be observed by NMR because the doublet splittings are not resolved in the corresponding elongation range.

The NMR slopes, P, have been measured at room temperature in samples with various CB grades and volume fractions and various sulfur/accelerator contents, that is, various cross-link densities. The obtained results are summarized in Table 3. The NMR slope, P, depends in a more sensitive way on the sulfur/accelerator content (i.e., on the cross-link density) than on the CB filler grade or volume fraction. Therefore, the effect of fillers, as measured by ^{2}H NMR experiments, is comparatively weak with respect to that of the bulk cross-link density. In particular, the slope, P, is not merely proportional to the filler content for a given CB grade. The effect of fillers on the average local chain stretching, as measured by NMR, has sometimes been interpreted to be that of an additional effective density of constraints at the filler surface.[46] Indeed, the observed linear variation could also be interpreted to be an effective change in cross-link density in the presence of fillers. However, the results presented here show that this additional contribution remains rather small with respect to the contribution arising from cross-links within the bulk of the matrix. However, samples reinforced with N326 and N358 CB grades, which have about the same specific surface area (but different structures), give different slopes. Finally, note that the bulk cross-link density may perhaps be quite inhomogeneous. This may in turn lead to variations among the elastomer matrices themselves in addition to those due to the presence of fillers with various volume fractions, structures, or both.

In regards to NMR in CB-filled systems, relatively few studies have been published. Some previously obtained results have shown that, unexpectedly, no significant amplification of orientation, as measured by ^{2}H NMR under strain, occurs in filled networks as compared with the pure matrix.[47] This was attributed to bad filler dispersion, with only a relatively small specific surface area of the fillers in contact with the matrix, thus leading to a relatively small fraction of the matrix effectively affected by the presence of fillers. However, it was shown by ^{1}H NMR that fillers have very little effect on the distribution of residual couplings in the relaxed state,[48] which shows that the contribution from additional effective cross-links due to interactions at the filler surfaces remains very small or even negligible. In contrast, it is observed here that the local strain (as reflected in the average orientation of the solvent molecules that diffuse within the mobile part of the matrix) is significantly affected in the presence of fillers. This shows that most of the matrix (not only the fraction in close contact to fillers) is affected, that is, submitted to amplified local strain. Such an effect on the NMR slopes was also observed in ref 46 in polyacrylate samples filled with well-dispersed spherical silica particles.

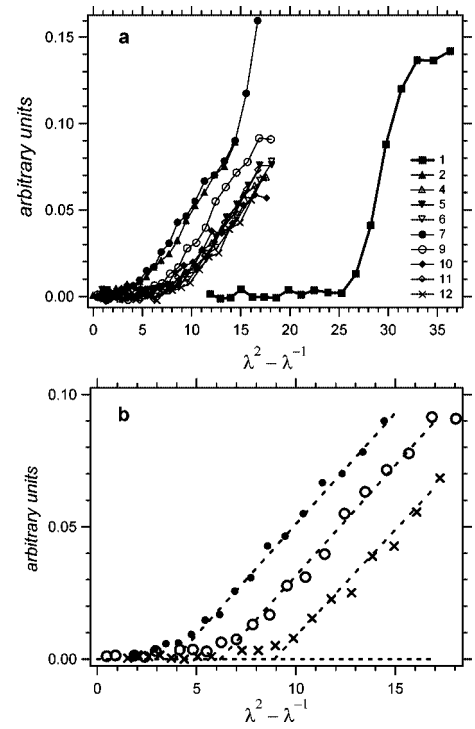

Figure 8. (a) Relative intensity of the 200 Bragg peak as a function of the elongation parameter, $\Lambda = \lambda^2 - \lambda^{-1}$, in the reference unfilled sample 1 and in the various reinforced samples. The measured intensity is proportional to the crystallinity ratio. In each sample, the onset of crystallization is measured as the intercept of the linearly extrapolated intensity curve with the baseline, as shown in the examples shown in (b) ●, sample 7; ○, sample 9; ×, sample 12.

C. Strain-Induced Crystallinity. Strain-induced crystallization has a strong effect on the mechanical behavior of elastomers. It leads to partial relaxation of the stress compared with the same hypothetically noncrystallizing matrix.[49−52] Therefore, it is important to check this here because polyisoprene may indeed strain crystallize, perhaps to a lesser extent than natural rubber, however. Additionally, comparing the onsets of crystallization in various samples may lead to an estimate of the local strain. The variation of the crystalline 200 Bragg peak intensity, I_{200} (measured as explained in Section IID), as a function of the elongation parameter $\Lambda = \lambda^2 - \lambda^{-1}$ is shown in Figure 8a in various samples.

In the nonreinforced sample, the curve is qualitatively similar to that obtained in vulcanized natural rubber.[49,53−55] Therefore, the behavior of the synthetic polyisoprene matrix used here is qualitatively quite similar to that of natural rubber in this respect.[56] In the present work, we will not discuss the absolute crystalline ratio but concentrate on only the onset of crystallinity λ_X (or equivalently Λ_X).

The first qualitative observation is that crystallinity starts at an elongation λ that is significantly smaller in reinforced samples than in the nonreinforced sample. The variation of crystallinity as λ increases differs in the nonreinforced sample and in reinforced samples. Even though it starts at much lower λ values, the subsequent increase is much slower in reinforced samples. This has already been observed in NR as well.[53] This very

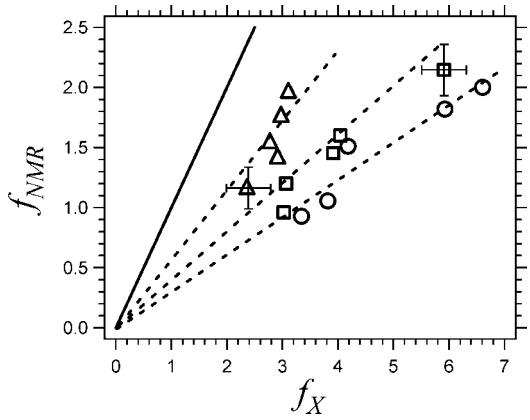

Figure 9. Amplification function, f_{NMR}, measured from ^2H NMR experiments as a function of the amplification function, f_X, measured from the onset of strain-induced crystallinity for samples with various cross-link densities and CB volume fractions. Three different CB grades are used: ○, N358; □, N326; △, N772. The plain line would correspond to $f_{NMR} = f_X$. Dashed lines are guides for the eye.

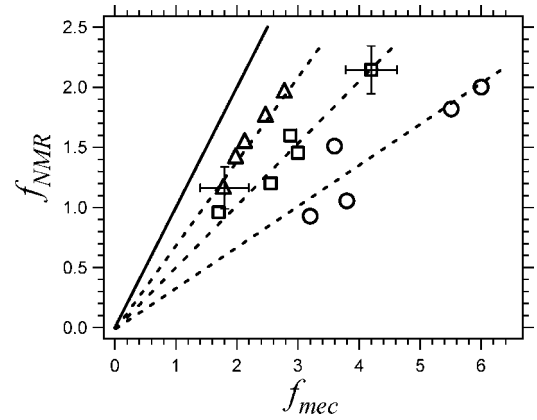

Figure 10. Amplification function, f_{NMR}, measured from NMR experiments as a function of the amplification function, f_{mec}, measured from mechanical experiments for samples with various cross-link densities and CB volume fractions. Three different CB grades are used: ○, N358; □, N326; △, N772. The plain line would correspond to $f_{NMR} = f_{mec}$. Dashed lines are guides for the eye.

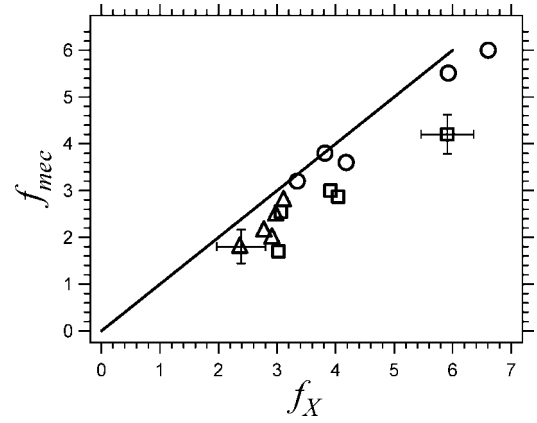

Figure 11. Amplification function, f_{mec}, measured from mechanical data as a function of the amplification function, f_X, measured from the onset of strain-induced crystallinity for samples with various cross-link densities and CB volume fractions. Three different CB grades are used: ○, N358; □, N326; △, N772. The plain line corresponds to $f_X = f_{mec}$.

progressive onset of crystallization observed in reinforced samples may be related to a distribution of local strains in the presence of fillers. The apparent onset would thus correspond to the most highly locally deformed areas within the rubbery matrix. (See the discussion below.) This makes the exact onset determination somehow difficult because of the limited sensitivity of peak intensity measurements. Figure 8b illustrates the way in which the onsets are determined from the curves shown in Figure 8a.

The values of the onset λ_X measured in all samples are reported in Table 3. The measured λ_X values confirm that the systems essentially do not crystallize in the elongation range investigated here in both mechanical and deuterium NMR measurements. X-ray diffraction data give the value of the strain amplification factor, f_X. The values of the strain amplification factor, f_X (as defined in eq 3), measured here at the stretching ratio, Λ_X, which corresponds to the onset of crystallization in each particular sample, are reported in Table 4.

The values obtained from crystallization data are on the same order as or somehow larger than those obtained through mechanical data. This has also already been observed in series of reinforced and nonreinforced NR samples.[49,53,55]

IV. Comparison of the Various Measurements and Discussion

The amplification functions, f, measured from mechanical data, deuterium NMR experiments, and measurements of the onset of strain-induced crystallization in the whole series of samples (with various cross-link densities and CB volume fractions) are compared with each other in Figures 9, 10, and 11. All factors, f, are computed by reference to the same unfilled reference sample. Different symbols are used to distinguish samples reinforced with different CB grades.

Before specifically discussing the results in Figures 9 to 11, let us make some general comments on the present results. The first point to emphasize is that different CB grades (i.e., CBs with either different primary particle sizes or different structures) give different reinforcement properties. Indeed, it is well recognized that the particle size, aggregate structure, and surface area of the carbon black are important parameters of reinforcement. It is shown here that the reinforcement level of the various CB grades is not simply related to the specific surface (i.e., to the overall quantity of interface present in the system). Indeed, CB grades N358 and N326 have about the same specific surface (as measured by N_2 absorption isotherms, Table 1) and give different reinforcement when added at the same volume fraction. This indicates that in the presence of complex structured filler aggregates, the volume density of interface area is not the primary (or certainly not the only) parameter needed to describe and interpret reinforcement properties.

We use a strain amplification representation to compare mechanical measurements with X-ray scattering and NMR measurements, which essentially measure the local strain. It is shown in Figure 5 that several distinct regimes occur successively in the mechanical response of the reinforced systems as the elongation amplitude increases.

First, in the Payne effect regime (below roughly 20% strain), the modulus (or equivalently, the amplification factor, f) drops quite steeply as the strain increases, which indicates that processes other than elastomeric elasticity are at play. Indeed, it has been proposed that reinforcement properties in the linear and Payne effect regime may be explained by the presence of a glassy layer around filler particles, related to long-range T_g shifts induced in the vicinity of a strongly interacting interface.[31,57] This has been specifically shown in a series of studies in model reinforced systems filled with monodisperse, well-distributed silica nanoparticles.[30,32,33] In the present systems in which filler aggregates have a complex structure and perhaps interact quite strongly, the stress may be transmitted in the linear

regime mainly by glassy bridges, which may then break progressively as the strain increases. Note that such T_g shifts have not yet been decisively measured in CB reinforced systems, particularly because of paramagnetism of carbon black, which broadens NMR lines in a way that cannot be conclusively distinguished from motional broadening.[44] Note also that microscopic mechanisms that are more complex than mere strain amplification and are related to reorganization of filler particles or aggregates may occur in the medium/large deformation range.[58]

The second regime, more specifically considered here, is very different from the Payne effect regime. It corresponds to a level of true stress up to 3 or 4 MPa in Figure 4 or equivalently to an intermediate range of deformation, defined roughly from $\lambda = 1.1$ to $\lambda = 2$ or 3 depending on the particular reinforced sample. (See Table 3.) In this regime, it is shown that mechanical data give a roughly constant or slightly increasing strain amplification factor, $f = \Lambda_m/\Lambda$ (eq 3). Then, it is not essentially different to consider the factor, f, or the stress amplification at a given elongation. In this regime, the level of reinforcement is relatively low, corresponding to f values from 2 to 5 in the various samples considered here. (See Table 4.) This is smaller than the reinforcement of the shear modulus measured in the linear regime, which is in the range of 3 to 10. (See Table 4.) Note that other CB-filled systems may have much higher reinforcement in the linear regime.[59]

Such moderate levels of reinforcement suggest that the response of the reinforced systems is essentially elastomeric in the full medium/large elongation range and at the temperature considered here or, in other words, that the modulus in the elastomer matrix is on the order of the elastomeric modulus of the pure matrix. This is an important result of this article, which validates experimentally geometrical approaches in this range of deformation. The values of the strain amplification factors obtained here are typically in the same range as those that may be computed from the model $f = 1 + 2.5\Phi/(1 - 2\Phi)$ proposed in ref 12, which gives $f = 1.96$ for $\Phi = 0.217$ and $f = 1.5$ for $\Phi = 0.143$. However, this model was tested in model systems with spherical fillers and is not intended to account for the differences induced by various CB morphologies. Here the more reinforcing CB gives an f value (with the same cross-link density as that of the reference) that is significantly higher than the predicted value. This is related to the large degree of interaction between filler aggregates, which occupy an effective spatial fraction larger than their mere volume fraction. However, the f_{NMR} value tends to be smaller than the predicted value, which indicates some degree of nonaffine reorganization of the fillers.

Here we compare the f values measured in each sample with different techniques, rather than quantitatively discuss the values obtained in various reinforced samples (with both different cross-link densities and/or different fractions and morphologies of CB fillers). In regards to the variation of the amplification factor, f, as a function of the elongation function, Λ, mechanical and NMR results are qualitatively consistent with each other, as previously mentioned above. However, the data obtained from various techniques, which are compared in Figures 9 to 11, deserve further discussion. In reinforced systems with homogeneous local strain and elastic modulus within the matrix, all three measurements should give the same value of the enhancement function, $f(\lambda)$, at a given macroscopic strain. Indeed, it is observed that the various measurements give f values that are well correlated and of the same order of magnitude. As is the case for the mechanical behavior, ^{2}H NMR and X-ray diffraction are sensitive to both the volume fraction, Φ, and the structure of the CB filler aggregates. This indicates that the higher level of mechanical reinforcement obtained with more reinforcing CB grades is effectively correlated to a higher level of local strain in the investigated regime.

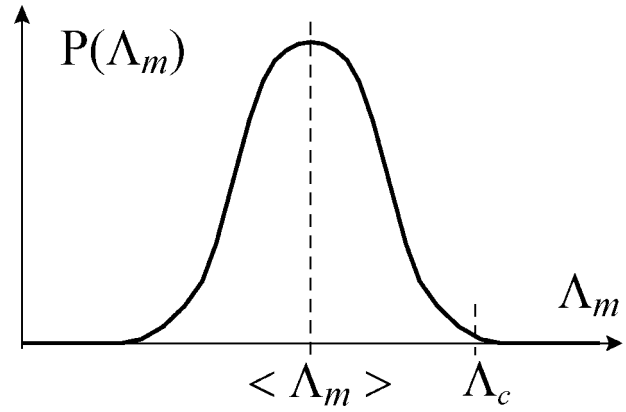

Figure 12. Sketch of a distribution $P_\Lambda(\Lambda_m)$ for the local strain parameter $\Lambda_m = \lambda_m^2 - \lambda_m^{-1}$ at a given macroscopic strain, Λ. $<\Lambda_m>$ is the average given by NMR measurements, Λ_c is the onset of strain induced crystallization. This illustrates the difference between NMR and X-ray measurements. (See Figure 9.)

The differences in the various measurements indicate some degree of inhomogeneity of the local strain in the presence of filler aggregates in reinforced samples. Indeed, because of the large distribution of distances between filler particles or aggregates, the deformation may perhaps be strongly nonaffine, and the local strain may vary considerably on the scale of filler particles or aggregates (typically 100 nm).

Let us first compare NMR data with measurements of the onset of crystallization (Figure 9). As shown in Figure 9, the NMR values are systematically about three times smaller than f_X. As discussed above, the matrix is likely to be mostly in the rubbery state at large elongation and, specifically, at the onset of crystallization. The differences between both measurements may thus essentially reflect inhomogeneities of the local strain. Let us describe the elongational strain by the parameter $\Lambda = \lambda^2 - \lambda^{-1}$, as done before, and assume that a distribution $P_\Lambda(\Lambda_m)$ of the local (microscopic) strain parameter, Λ_m, is associated with the macroscopic (applied) strain, Λ. (See Figure 12.) According to eq 2, neglecting local variations of the elastic modulus and assuming fast solvent diffusion, ^{2}H NMR measurements give the average order parameter $S(\Lambda) = \nu/N \int P_\Lambda(\Lambda_m)\Lambda_m \, d\Lambda_m = \nu/N<\Lambda_m>$; that is, NMR gives access to the average local strain parameter within the matrix. Note that we have supposed here that the local strain is essentially uniaxial with a variable elongation ratio, Λ_m, thus neglecting 3D effects. However, crystallization occurs first in the most stretched zones, that is, as the right-hand side of the distribution $P_\Lambda(\Lambda_m)$ reaches the onset Λ_c (as shown in Figure 12). The crystallization curve would then be given by $X(\Lambda) = \int X_0(\Lambda_m)P_\Lambda(\Lambda_m) \, d\Lambda_m$, where $X_0(\Lambda)$ describes the crystallization curve in the pure matrix. This may also account for the more progressive onset of crystallization in reinforced samples as compared with the reference sample observed in Figure 8, already mentioned in Section IIIC, which is then a further experimental indication of an inhomogeneous strain level in the reinforced matrix.

The difference between f_{NMR} and f_X shown in Figure 9 thus reflects the width of the local strain distribution $P_\Lambda(\Lambda_m)$. Figure 9 shows that this difference depends on the grade of the CB used as reinforcing fillers. It is all the more pronounced as a more reinforcing CB is used. This is an important result of this article. It indicates that more reinforcing CB grades (finer, more structured, or both) are associated with a broader distribution of the local strain or, equivalently, with a higher level of stress inhomogeneity. This may be related to a broader distribution of interparticle (or interaggregate) distances in the presence of

the more reinforcing CB aggregates. Indeed, this distribution of distances may be one key feature that determines the different levels of reinforcement. Also, Figure 9 indicates a way to discriminate the effect of filler morphology and cross-link density on reinforcement. Also, note that part of the local inhomogeneity of the samples may come from the presence of zinc oxide aggregates.[60]

Note that a distribution of local strain on a mesoscopic scale was explicitly computed using the 'virtual rubber' approach at 15% external strain in a CB-filled rubber.[16,17,61] A trimodal distribution was found, with an "occluded" region (relative weight 7%) having very small local strain, a majority (60%) region at 15% strain, and a region (33%) with strain amplified four to five times. It may be considered that the NMR value reflects the majority region or the overall average of the local strain distribution, whereas the crystallinity onset reflects the strain amplified region. Therefore, the values obtained here are in qualitative agreement with this model. However, the present results do not allow us to discriminate a multimodal distribution of local strain, as computed in ref 16 from a distribution exemplified in Figure 12. Note that in the "virtual rubber" approach, the constitutive law for the rubbery matrix is supposed to be the same as that for the pure matrix. Therefore, the comparison that is done here is a further indication that the elastomer matrix is indeed in the rubbery state in the elongation range considered herein.

Let us now compare NMR data with mechanical measurements. As shown in Figure 10, the function f, as measured by NMR, is 2 to 3 times smaller than the value f_{mec} given by mechanical data. This difference indicates that mechanical properties are not related to the average local chain stretching only. Some zones that participate in the NMR averaging process do not participate in the stress transmission; conversely, a fraction of the stress is transmitted through zones in the material, namely, fillers, which do not participate in the NMR averaging. Let us consider now the correlation between mechanical and X-ray measurements (Figure 11). Values of f_{mec} are well correlated to f_X, which was already observed in various reinforced NR samples.[49,55] This correlation indicates that the parts of the elastomer matrix that predominantly contribute to the stress are those that crystallize first, that is, those with the larger local strain.

V. Conclusions

We have studied polyisoprene elastomers reinforced with carbon black aggregates of various grades by combining mechanical measurements and techniques that give access to the microscopic strain within the elastomer matrix, namely, ^{2}H NMR, which measures local chain stretching in the elastomer matrix, and X-ray diffraction, which gives strain-induced crystallization. We have investigated the medium/large deformation regime beyond the Payne effect and below the self-reinforcement due to strain-induced crystallization.

We have shown that NMR experiments and measurements of the onset of crystallization are indeed sensitive to the different degrees of reinforcement observed according to the various CB grades (and volume fractions). The measurements show a very good correlation between macroscopic (mechanical) and microscopic (NMR, crystallization) measurements. This indicates that the techniques used here are valuable techniques for characterizing such systems, in which filler aggregates have complex morphologies and dispersion states. The correlation between the various results suggests that the mechanical response is essentially elastomeric in the elongation regime investigated, in contrast with the Payne effect regime. When quantitatively comparing the results of both macroscopic and microscopic measurements, there are some discrepancies: the local strain measured via NMR experiments is systematically smaller than that inferred from large amplitude mechanical measurements and from the onset of crystallization. NMR measurements give an average of the local strain within the elastomer matrix, whereas crystallization first occurs in the most strained parts of the matrix. The observed difference is thus related to the distribution of local strain, or nonaffinity, within the matrix. This indicates the presence of some degree of inhomogeneity in the elastomer matrix. The degree of strain inhomogeneity depends on the CB grade, which is used to reinforce the elastomer. It is larger for a more reinforcing CB. This indicates that reinforcement is correlated to the local strain (or stress) inhomogeneity. This inhomogeneity may be related to the distribution of distances within the systems.

Acknowledgment. This work was done at the Laboratoire de Physique des Solides, CNRS/Universit Paris-Sud, Orsay, France. We thank Laboratoire Léon Brillouin (CNRS/CEA, Saclay, France) for allowing us access to the ARES rheometer, which was used to measure the shear moduli in the linear regime. We thank Manufacture Francaise des Pneumatiques Michelin, Ladoux, France, for providing the samples.

References and Notes

(1) Wang, M. J. *Rubber Chem. Technol.* **1998**, *71*, 520.
(2) Kraus, G. *Reinforcement of Elastomers*; Interscience Publishers: New York, 1965; p 156.
(3) Nielsen, L. E.; Landel, R. F. *Mechanical Properties of Polymers and Composites*; Marcel Dekker: New York, 1994.
(4) Medalia, A. I. *J. Colloid Interface Sci.* **1970**, *32*, 115.
(5) Medalia, A. I. *Rubber World* **1973**, *168*, 49.
(6) Medalia, A. I. *Rubber Chem. Technol.* **1978**, *51*, 437.
(7) Witten, T. A.; Rubinstein, M.; Colby, R. H. *J. Phys. II* **1993**, *3*, 367–383.
(8) Guth, E.; Gold, O. *J. Appl. Phys.* **1945**, *16*, 20.
(9) Bueche, F. *J. Appl. Polym. Sci.* **1960**, *4*, 107.
(10) Bueche, F. *J. Appl. Polym. Sci.* **1961**, *5*, 271.
(11) Bueche, F. In *Reinforcement of Elastomers*; Kraus, G., Ed.; John Wiley and Sons: New York, 1965; p 1.
(12) Westermann, S.; Kreitschmann, M.; Pyckhout-Hintzen, W.; Richter, D.; Straube, E.; Farago, B.; Goerigk, G. *Macromolecules* **1999**, *32*, 5793.
(13) Westermann, S.; Pyckhout-Hintzen, W.; Richter, D.; Straube, E.; Egelhaaf, S.; May, R. *Macromolecules* **2001**, *34*, 2186.
(14) Reichert, W. F.; Goritz, D.; Duschl, E. J. *Polymer* **1993**, *34*, 1216.
(15) Fukahori, Y. *Rubber Chem. Technol.* **2007**, *80*, 701.
(16) Akutagawa, K.; Yamaguchi, K.; Yamamoto, A.; Heguri, H.; Jinnai, H.; Shinbori, Y. *Rubber Chem. Technol.* **2008**, *81*, 182.
(17) Ikeda, K.; Kato, A.; Shimanuki, J.; Kohjiya, S.; Tosaka, M.; Poompradub, S.; Toki, S.; Hsiao, B. S. *Rubber Chem. Technol.* **2007**, *80*, 251.
(18) Fukahori, Y.; Seki, W. *J. Mater. Sci.* **1993**, *28*, 4471.
(19) Litvinov, V. M.; Steeman, P. A. M. *Macromolecules* **1999**, *32*, 8476.
(20) Maier, P. G.; Goeritz, D. *Kautsch. Gummi Kunstst.* **1996**, *49*, 18.
(21) Payne, A. R. *J. Appl. Polym. Sci.* **1965**, *9*, 1073.
(22) Kraus, G. *J. Appl. Polym. Sci.: Appl. Polym. Symp.* **1984**, *39*, 440.
(23) Heinrich, G.; Klüppel, M.; Vilgis, T. A. *Curr. Opin. Solid State Mater. Sci.* **2002**, *6*, 195.
(24) Klüppel, M.; Schuster, H. R.; Heinrich, G. *Rubber Chem. Technol.* **1997**, *70*, 243.
(25) Gerspacher, M.; O'Farrell, C. P. *Kautsch. Gummi Kunstst.* **1998**, *51*, 488.
(26) Hueber, G.; Vilgis, T. A. *Kautsch. Gummi Kunstst.* **1999**, *52*, 102.
(27) Stacer, R. G.; Huebner, C.; Husband, D. M. *Rubber Chem. Technol.* **1990**, *63*, 488. *49*, 18.
(28) Klüppel, M. *Adv. Polym. Sci.* **2003**, *164*, 1–86.
(29) Long, D.; Lequeux, F. *Eur. Phys. J. E* **2001**, *4*, 371.
(30) Berriot, J.; Montès, H.; Lequeux, F.; Long, D.; Sotta, P.; Monnerie, L. *Europhys. Lett.* **2003**, *64*, 50.
(31) Merabia, S.; Sotta, P.; Long, D. *Eur. Phys. J. E* **2004**, *15*, 189.
(32) Berriot, J.; Lequeux, F.; Monnerie, L.; Montès, H.; Long, D.; Sotta, P. *J. Non-Cryst. Solids* **2002**, *307*, 719.
(33) Berriot, J.; Montès, H.; Lequeux, F.; Long, D.; Sotta, P. *Macromolecules* **2002**, *35*, 9756.
(34) Berriot, J.; Lequeux, F.; Montès, H.; Pernot, H. *Polymer* **2002**, *43*, 6131.
(35) Robertson, C. G.; Lin, C. J.; Rackaitis, M.; Roland, C. M. *Macromolecules* **2008**, *41*, 2727.

(36) Sotta, P.; Deloche, B. *Macromolecules* **1990**, *23*, 1999.
(37) Sotta, P. *Macromolecules* **1998**, *31*, 3872.
(38) Rieker, T. P.; Misono, S.; Ehrburger-Dolle, F. *Langmuir* **1999**, *15*, 914.
(39) Ehrburger-Dolle, F. *Carbon* **1996**, *34*, 828–831.
(40) Deloche, B.; Sotta, P. Deuterium NMR in Rubbery Materials. In *Spectroscopy of Rubbers and Rubbery Materials*; Litvinov, V. M., De, P. P.; Rapra Technology, Ltd.: Shawbury, U.K., 2000; p 557.
(41) Sotta, P.; Deloche, B.; Herz, J. *Polymer* **1988**, *29*, 1171.
(42) Trabelsi, S.; Albouy, P. A.; Rault, J. *Macromolecules* **2003**, *39*, 7624.
(43) Mitchell, G. R. *Polymer* **1984**, *25*, 1562.
(44) Ekanayake, P.; Menge, H.; Schneider, H.; Ries, M. E.; Brereton, M.; Klein, P. G. *Macromolecules* **2000**, *33*, 1807.
(45) In computing the value of the quadrupolar constant, we suppose that cyclohexane molecules lie with the C6 ring parallel to the magnetic field, B_0, so as to intercept zero magnetic flux. Rotation of the molecule around its axis averages the quadrupolar tensors parallel to C−D bonds along the molecule axis with a reduction factor on the order $^1/_2$. Rotation of the molecules around the magnetic field direction (which coincides with the stretching direction and is a symmetry axis in this problem) further averages the tensor along the magnetic field direction with a factor of $^1/_2$. The magnitude of the resulting quadrupolar tensor is therefore $\omega_Q = 125 \times (^1/_2) \times (^1/_2) \approx 31$ kHz (the doublet splitting is $2\omega_Q$).
(46) Berriot, J.; Martin, F.; Montès, H.; Monnerie, L.; Sotta, P. *Polymer* **2003**, *44*, 1437.
(47) Baumann, K.; Gronski, W. *Prog. Colloid Polym. Sci.* **1992**, *90*, 97.
(48) Saalwächter, K.; Klüppel, M.; Luo, H.; Schneider, H. *Appl. Magn. Reson.* **2004**, *27*, 401.
(49) Rault, J.; Marchal, J.; Judeinstein, P.; Albouy, P. A. *Macromolecules* **2006**, *39*, 8356.
(50) Flory, P. J. *J. Chem. Phys.* **1947**, *15*, 397.
(51) Miyamoto, Y.; Yamao, H.; Sekimoto, K. *Macromolecules* **2003**, *36*, 6462.
(52) Toki, S.; Sics, I.; Hsiao, B. S.; Murakami, S.; Tosaka, M.; Poompradub, S.; Ikeda, Y.; Kohjiya, S. *Macromolecules* **2005**, *38*, 7064.
(53) Trabelsi, S.; Albouy, P. A.; Rault, J. *Rubber Chem. Technol.* **2004**, *77*, 303.
(54) Chenal, J.-M.; Chazeau, L.; Guy, L.; Bomal, Y.; Gauthier, C. *Polymer* **2007**, *48*, 1042.
(55) Chenal, J.-M.; Gauthier, C.; Chazeau, L.; Guy, L.; Bomal, Y. *Polymer* **2007**, *48*, 6893.
(56) Toki, S.; Sics, I.; Ran, S.; Liu, L.; Hsiao, B. S.; Murakami, S.; Tosaka, M.; Kohjiya, S.; Poompradub, S.; Ikeda, Y.; Tsou, A. H. *Rubber Chem. Technol.* **2004**, *77*, 317.
(57) Merabia, S.; Sotta, P.; Long, D. R. *Macromolecules* **2008**, *41*, 8252.
(58) Long, D.; Sotta, P. *Macromolecules* **2006**, *39*, 6282.
(59) Payne, A. R. *J. Appl. Polym. Sci.* **1963**, *7*, 873.
(60) Hidehiko Dohi, H.; Shin Horiuchi, S. *Polymer* **2007**, *48*, 2526.
(61) Jinnai, H.; Shinbori, Y.; Kitaoka, T.; Akutagawa, K.; Mashita, N.; Nishi, T. *Macromolecules* **2007**, *40*, 6758.

MA900006Y